AD-A179 725 INTEGRATION OF STATISTICAL AND PHYSICAL MODELS OF SHORT FATIGUE CRACK GRO..(U) ROCKWELL INTERNATIONAL THOUSAND OAKS CA SCIENCE CENTER B N COX ET AL. FEB 87 SC5410-AR 1/1

UNCLASSIFIED AFOSR-TR-87-0397 F49620-85-C-0034 F/G 20/11 NL

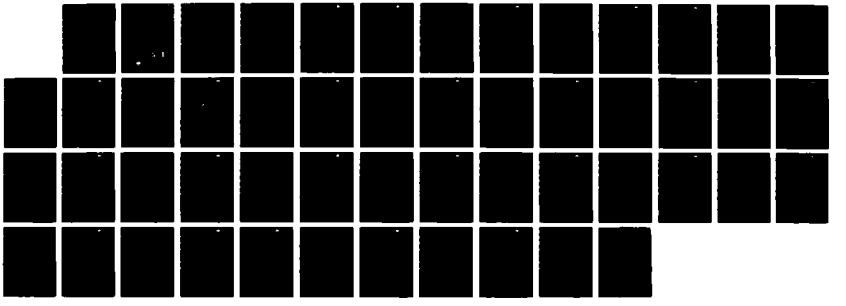

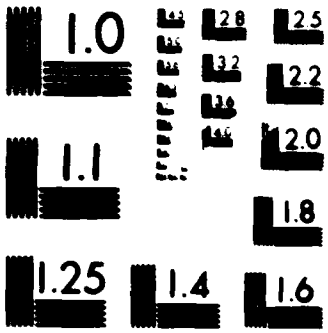

AD-A179 725

SC5418.AR

SC5418.AR
Copy No. 3

AFOSR-TR- 87-0397

INTEGRATION OF STATISTICAL AND PHYSICAL MODELS OF SHORT FATIGUE CRACK GROWTH

ANNUAL REPORT NO. 2 FOR THE PERIOD January 15, 1986 through January 14, 1987

CONTRACT NO. F49620-85-C-0034

Prepared for

AFOSR/NA
Directorate of Aerospace Sciences
Building 410
Bolling AFB, DC 20332

B.N. Cox
W.L. Morris
Principal Investigators

FEBRUARY 1987

Approved for public release; distribution unlimited

Rockwell International
Science Center

UNCLASSIFIED
SECURITY CLASSIFICATION OF THIS PAGE

ADA179725

REPORT DOCUMENTATION PAGE

1a. REPORT SECURITY CLASSIFICATION UNCLASSIFIED	1b. RESTRICTIVE MARKINGS
2a. SECURITY CLASSIFICATION AUTHORITY	3. DISTRIBUTION/AVAILABILITY OF REPORT Approved for public release; distribution unlimited
2b. DECLASSIFICATION/DOWNGRADING SCHEDULE	
4. PERFORMING ORGANIZATION REPORT NUMBER(S) SC5418.AR	5. MONITORING ORGANIZATION REPORT NUMBER(S) AFOSR-TR- 87-0397
6a. NAME OF PERFORMING ORGANIZATION ROCKWELL INTERNATIONAL Science Center 6b. OFFICE SYMBOL (If Applicable)	7a. NAME OF MONITORING ORGANIZATION AFOSR
6c. ADDRESS (City, State, and ZIP Code) 1049 Camino Dos Rios Thousand Oaks, CA 91360	7b. ADDRESS (City, State and ZIP Code) BLDG 410 BAFB DC 20332
8a. NAME OF FUNDING SPONSORING ORGANIZATION AFOSR/NA 8b. OFFICE SYMBOL (If Applicable) NA	9. PROCUREMENT INSTRUMENT IDENTIFICATION NUMBER CONTRACT NO. F49620-85-C-0034
8c. ADDRESS (City, State and ZIP Code) Directorate of Aerospace Sciences, Building 410 Bolling AFB, DC 20332	10. SOURCE OF FUNDING NOS. PROGRAM ELEMENT NO. 61102F; PROJECT NO. 2302; TASK NO. B2; WORK UNIT NO.
11. TITLE (Include Security Classification) INTEGRATION OF STATISTICAL AND PHYSICAL MODELS OF SHORT FATIGUE CRACK GROWTH	
12. PERSONAL AUTHOR(S) Cox, B.N., Morris, W.L.	
13a. TYPE OF REPORT Annual Report No. 2	13b. TIME COVERED FROM 01/15/86 TO 01/14/87
14. DATE OF REPORT (Yr., Mo., Day) 1987, FEBRUARY	15. PAGE COUNT 40
16. SUPPLEMENTARY NOTATION	

17. COSATI CODES		
FIELD	GROUP	SUB. GR

18. SUBJECT TERMS (Continue on reverse if necessary and identify by block number)

19. ABSTRACT (Continue on reverse if necessary and identify by block number)

This report describes work conducted under the second year of a program of integrating physical and statistical models of small fatigue crack growth.

A computer program has been written that generates Monte Carlo simulations of small fatigue crack growth. The simulations allow predictions of the statistics of growth given postulated or empirical laws defining the effects of local stochastic microstructure. Variations in crack shape and irregularity of the crack front, correlations between surface and subsurface growth rates, and the probability and effects of part or all of the crack front being temporarily arrested at grain boundaries can all be calculated. The simulation of embedded and surface cracks of irregular shape is made feasible by the development of approximate, fast algorithms for estimating variations in the Mode I stress intensity factor, K around an irregular plane crack.

KsubI

20. DISTRIBUTION/AVAILABILITY OF ABSTRACT UNCLASSIFIED/UNLIMITED ☐ SAME AS RPT. ☒ DTIC USERS ☐	21. ABSTRACT SECURITY CLASSIFICATION UNCLASSIFIED
22a. NAME OF RESPONSIBLE INDIVIDUAL Major George Haritos	22b. TELEPHONE NUMBER (Include Area Code) 202-767-4912 22c. OFFICE SYMBOL NA

DD FORM 1473, 83 APR EDITION OF 1 JAN 73 IS OBSOLETE

UNCLASSIFIED (cont'd)
SECURITY CLASSIFICATION OF THIS PAGE

A

19. Abstract (Continued)

The simulations provide a convenient way of generating large, detailed, synthetic data bases for small crack growth under diverse conditions. These data bases can then be used in lieu of experimental data to test simpler, but more efficient and robust probabilistic models of crack growth such as the one developed in the first year of this program. They also provide the theoretical framework required for understanding the role of fluctuations in the shape of small cracks in determining their rate of growth. By comparing the predicted statistics of the shape of small cracks with experimental data such as from striations, postulated laws of the dependence of growth rate on stochastic microstructure can be tested.

TABLE OF CONTENTS

LIST OF FIGURES

LIST OF FIGURES

1.0 INTRODUCTION

This report describes work in the second year of the program "Integration of Statistical and Physical Models of Short Fatigue Crack Growth," Contract No. F49620-85-C-0034 with AFOSR. The second year of this program (January 15, 1986 to January 14, 1987) has now been completed.

1.1 Note on Nomenclature

It has rightly become popular in the last year or two to distinguish carefully between cracks whose size is small relative to the microstructure in both dimensions or just one dimension. Cracks that are small in just one dimension, e.g., a through-crack in a notched plate that has not yet propagated very far, are termed "short". Cracks that are small in both dimensions, e.g., a surface-breaking crack, for which the aspect ratio of depth to surface length is typically ~ 0.4, are termed "small". The distinction is especially important when considering statistical aspects of crack growth. For a short crack, statistical fluctuations may be averaged out over the comparatively long dimension of the crack (e.g., the thickness of the plate for a short through-crack), and therefore not manifested in fatigue lifetime. In a small crack, which is often the form of a naturally initiated fatigue crack, there is no such averaging; and one generally expects statistical fluctuations generated by the stochastic microstructure to cause much greater fluctuations in lifetimes. In this report, this modern terminology is respected. Most of the probabilistic models described herein were developed specifically to address small cracks. Note, however, that with little modification they could also be applied to short cracks.

1.2 Summary of the First Year's Work

In the first year of the program, a probabilistic model was formulated that drew a direct link between stochastic microstructures and the statistics of measured growth rates. The model was formulated as a semi-Markov chain in which the underlying Markov process describes the evolution of a growth control variable as an explicit function of crack length. The growth control variable may be assigned a variety of interpretations, depending on the mechanisms known to control growth in any application. Elapsed fatigue cycles and the distribution of times to failure are calculated by invoking

an empirical or postulated law of growth rate. The law may, and usually does, contain parameters that are evaluated by calibration against available statistical data, which guarantees a minimum level of accuracy of the model's predictions. On the other hand, the freedom of interpretation of the growth control variable allows the model to be applied to systems with diverse mechanisms of damage accumulation, and the structure of the model allows physical understanding of those mechanisms to be transferred directly to enhanced accuracy of predictions. This work has been described in detail in the first annual report[1] and in the open literature.[2]

The model may also be regarded as a research tool, a dual role that has been well illustrated by the first application, which was to data for Ti 6Al-2Sn-4Zr-6Mo.[1,3] Model-based analysis of these data led to the following conclusion. Fluctuations in the instantaneous rate of growth of the surface tips of a small surface-breaking crack in Ti 6-2-4-6 are sensitive only to the microstructure of the material at or very near the surface. They do not depend on the sizes of the grains lying on the crack front beneath the surface. This conclusion is based solely yet firmly on a model-based statistical analysis of the dependence of the magnitude of fluctuations in crack tip velocity on crack length. It is an important conclusion for the rest of this work, because when such a state of affairs holds, the statistics of the growth of surface cracks can be described by a model that considers surface and near-surface phenomena only. However, the data considered for Ti 6-2-4-6 were predominantly for cracks that spanned ~ 5-20 grains, and it is unlikely that the same conclusion will still be valid for cracks that span only one or two grains. For these smallest of cracks, there ought to be a strong correlation between subsurface and surface growth rates. The expected transition between these two regimes has been one of the subjects addressed in the second year's work.

1.3 Generation of a Synthetic Data Base

With a basic, flexible probabilistic model thus established, the next task in the program was to generate a large synthetic data base against which the model could be tested. This has been the major accomplishment of the second year. A computer program has been written that carries out Monte Carlo simulations of the growth of small cracks through a stochastic microstructure. The Monte Carlo simulations allow the consideration of any given set of laws of crack growth. The simulation is as realistic as feasible, treating a fully two-dimensional crack bounded by an arbitrarily irregular crack

front. The crack may be either embedded or surface breaking. A great variety of salient statistics are gathered from the simulations, representing a rich background of physical detail against which predictive models can be appraised.

1.4 Outline of This Report

A substantial task that occupied the first few months of the second year was the development of more rigorous algorithms and software than were used in the first year[1] to perform calibration of the probabilistic model against field or laboratory data. This work is reported in Section 2 and illustrated by the application to the Ti 6-2-4-6 data of Ref. 3. The computational and physical details of the Monte Carlo simulations are reported in Section 3, including a new, simple algorithm for rapid estimation of the mode I stress intensity factor K_I around an irregular plane crack. In Section will also be found a discussion of the gathering of useful statistics from the Monte Carlo simulations. Work planned for the third year of the contract is described in Section 4.

2.0 CALIBRATION OF THE PROBABILISTIC MODEL

In this section, the more rigorous procedure for calibrating the probabilistic model developed in the first year will be reported. The calibration amounts to evaluation of certain parameters embodied in a postulated or empirical law of growth by selecting the best fit to experimental data. The more rigorous procedure has led to some slight modifications of the conclusions reported in Ref. 1, as described below. For ease of explanation, the procedure is presented in terms of an analysis of data for short cracks in Ti 6-2-4-6, as in Refs. 1 and 3.

2.1 The Role of the Calibration

The probabilistic model of small crack growth was formulated in terms of a growth control variable, u, that is a random variable.[1,2] The variable u is not always well suited to direct experimental measurement. For example, in the model of roughness-induced closure used to analyze the data for Ti 6-2-4-6, u corresponds to the average size of the grains lying at or near the crack front,[1,3] which would be very tedious to measure for surface grains, and impossible for subsurface grains by any nondestructive technique. In such cases, the statistics of u are known solely from theory. As indicated in the block diagram of Fig. 1, theory must in such cases provide a model of evaluating the Probability Transition Matrices (PTMs) of u, which define the probability that u should take one value at a certain discrete value of crack length, given that it had another value at the immediately prior discrete value of crack length. The calculation of the PTMs usually relies on a simple physical or geometrical model of the stochastic microstructure constituting the material under consideration. Such a model is called a "u-model" for brevity. Two examples of u-models were presented in the analysis of the Ti 6-2-4-6 data.[1,3] One u-model (Model 1) was based on the premise that fluctuations in the velocities of the visible surface crack tips are influenced only by the neighboring surface grain structure; and the other (Model 2) on the premise that the velocity fluctuations depend on some average of the grain structure lying along the entire crack front. As in these examples, the u-models are frequently derived from purely geometrical considerations of the stochastic microstructure.

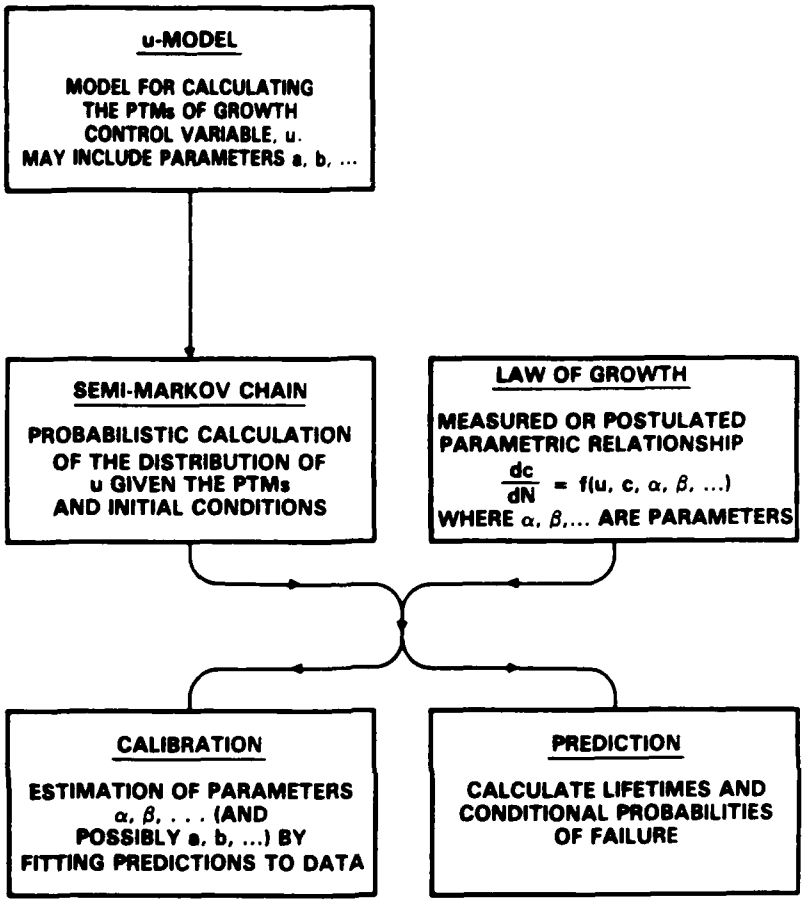

Fig. 1 Block diagram of the genesis and calibration of a probabilistic model of short crack growth.

2.2 Model Validation - The Distribution of Velocities

The connection between the growth control variable u and measurable crack velocities, and hence lifetimes, is expressed by some empirical or postulated law of crack growth. In the present example of short crack growth in Ti 6-2-4-6, where the dominant mechanism controlling growth rate is fracture surface roughness, the form of the law of crack growth is[4]

$$2\frac{dc}{dN} \equiv v(c,u) = A[-\alpha\, u + 1.12\, \sigma_{max} \sqrt{2c}]^{\beta} \quad , \tag{1}$$

where 2c is the visible surface crack length; A, α, and β are the parameters to be evaluated; u is the growth control variable appearing as a continuous variable; and σ_{max} is the applied fully reversed cyclic load amplitude. In the original derivation of this law, the variable u represented the measured crack opening displacement at zero load. The law was established by fitting crack opening data for a moderately large number of individual cracks growing through grains whose sizes were individually measured and recorded. In fact, the measured CTODs have an approximately constant average for cracks of length $\geq$ 100 μm, but fall away for shorter cracks, and must vanish at zero crack length.[4] Since the velocity data continue to show considerable scatter (see Fig. 2) for even the shortest cracks, it may well be that fracture surface roughness is indeed not the only growth control mechanism, especially for cracks of length $\leq$ 50 μm. However, since only the shortest cracks would be strongly affected, Eq. (1) as it stands is sufficiently true to the original study for the present purposes.

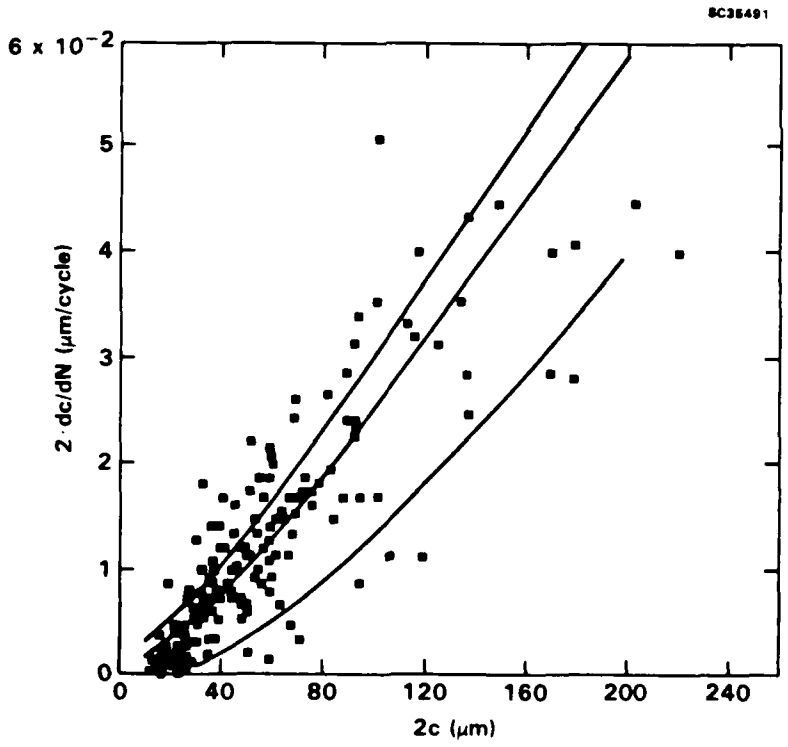

Fig. 2 The crack growth data of Ref. 4 for Ti 6-2-4-6. The three curves represent the velocity corresponding to the average value of u and two bounds that should encompass 70% of the data calculated using Model 1 of Refs. 1 and 3 (n = 3).

The variable u is, of course, a random variable, whose distribution at any crack length is given by Eq. (5) of Ref. 2, namely,

$$F_u^{(k)}(u_j^{(k)}) = \sum_{i<j} \pi_j^{(k)} \tag{2}$$

where $F_u^{(k)}(u_j^{(k)})$ is the cumulative probability distribution (cpd) for the variable u in terms of discretized values $u_j^{(k)}$; and $\pi_j^{(k)}$ is the probability, calculated from the PTMs prescribed by the u-model, that u should take the discrete value $u_j^{(k)}$ at the discrete value of crack length $2c_k$. For the following model validation, $F_u(u|c)$, a cpd for the continuous variable u at any crack length 2c, was generated by a numerical smoothing algorithm and interpolation over $\{2c_k\}$. $F_u(u|c)$ is determined almost entirely by the PTMs $\underline{P}^{(m)}$, which in the present application are prescribed by the u-models "Model 1" or "Model 2" of Refs. 1 and 3. It is not strongly influenced by the assumed initial distribution $\underline{\pi}^{(0)}$. (General note: in other applications, this may not always be the case.)

Equation (1) may be regarded as a deterministic, one-to-one relationship between u and v at fixed crack length, 2c, and it possesses the inverse relationship

$$u = u(v,c) \quad , \tag{3}$$

which expresses u as a strictly monotonically decreasing function of v. The cpd for crack velocities, $F_v(v|c)$, may therefore be written

$$F_v(v|c) = 1 - F_u(u(v,c)|c) \quad . \tag{4}$$

The validation procedure consists of finding the parameters A, β, and α in Eq. (1) that cause $F_v(v|c)$ to most closely resemble the experimental distributions of 2dc/dN at all crack lengths given the model-based distributions $F_u(u|c)$.

There are various ways this optimization task can be carried out. In this work, a modification of a method considered by Fertig[5] was employed. Given values of the parameters A, β, and α, Eq. (3) implies a value, u_i, of the growth control variable for each experimental data pair $(2c_i, V_i)$. Let there be N_d such data pairs and implied values u_i. With each value u_i may be associated the random variable

$$y_i = F_u(u_i|c_i). \tag{5}$$

For a valid model and an infinite data set, y_i must be uniformly distributed over the interval [0,1]. The optimum values of the parameters A, β, and α may be found in principle by minimizing the Cramer-von Mises test function

$$S = \sum_i \left[y_i - \frac{i}{N_d + 1}\right]^2 , \tag{6}$$

with the y_i previously sorted into ascending order. For the given, finite data set, a modification of this procedure was used to avoid finding spurious, local minima of $S(A,\beta,\alpha)$ with the available minimization algorithm. The data $\{(2c_i, V_i)\}$ were divided amongst p equal subsets, Ω_k, in such a way that

$$2c_i < 2c_j \text{ if } i \in \Omega_k,\ j \in \Omega_{k'},\ \text{and } k < k'. \tag{7}$$

The corresponding y_i of Eq. (5) were ordered within each subset, and the minimization was carried out for the sum

$$S = \sum_k \left(\sum_{i \in \Omega_k} \left[y_i - \frac{i}{N_k + 1}\right]^2 \right), \tag{8}$$

where N_k is the number of data points in Ω_k. The resulting values of A, β, and α were found to be essentially independent of p for $2 \le p \le 5$.

The results of the procedure for optimization are summarized for Model 1 of Refs. 1 and 3 (where dc/dN is determined by surface microstructure only) in Table 1. The three cases n = 1,3, and 10 are shown, where n is the number of surface grains in the wake of the crack tip supposed to influence the fluctuations in its velocity. There are some differences in the corresponding parameters A, β, and α, but not enough to distinguish between the merits of the three cases. In Fig. 2, the three functions, v(c,Eu), $v(c,u^+)$, and $v(c,u^-)$ have been superimposed (solid lines) on the data for the case n = 3. $u^{\pm}$ are the values of u defined by

$$F_u(u^+|c) = 0.85$$

and $$F_u(u^-|c) = 0.15, \quad (9)$$

so that the outer curves should contain 70% of the data points. The equivalent curves for n = 1 and n = 10 show no significant differences to the case n = 3. One cannot discriminate between the merits of these three cases by their ability to reproduce the average or the scatter in 2dc/dN. Note that this conclusion is different to that reported in Ref. 1, which was based on a simplistic validation procedure.

Table 1

Optimal Parameters A, β, and α and Correlation Length λ^+ for Variants of Model 1

n(a)	A (μm/cycle) x 10^3	β	α(b)	λ^+ (μm)
1	0.540	2.02	0.359	< 10
3	0.562	2.05	0.304	14
10	0.516	2.16	0.377	60

(a) The instantaneous value of dc/dN is assumed to be controlled by the average of the distances between the last n deflections suffered by the visible surface crack.

(b) The values given for α are obtained when u is expressed in μm and $\sigma_{max}\sqrt{2c}$ in MPa-$m^{1/2}$ in Eq. (1).

On the other hand, Model 2 of Ref. 3 (where dc/dN is determined by the microstructure along the entire crack front) is clearly incorrect. In Fig. 3, the same curves, v(c,Eu), $v(c,u^+)$, and $v(c,u^-)$ are plotted against the data using the optimized parameters of Model 2 and the corresponding distributions F_u. While the predicted average growth is acceptable, given the thinness of the data at lengths > 100 μm, the scatter in 2dc/dN is clearly not reproduced. To highlight this failure, the rmsd found experimentally in 2dc/dN has been compared in Fig. 4 with the rmsd calculated according to Model 1 (n = 3) and Model 2. The experimental values were estimated by grouping the data $(2c_i, V_i)$ into ten bins b_j centered around lengths $2c'_j$, and finding

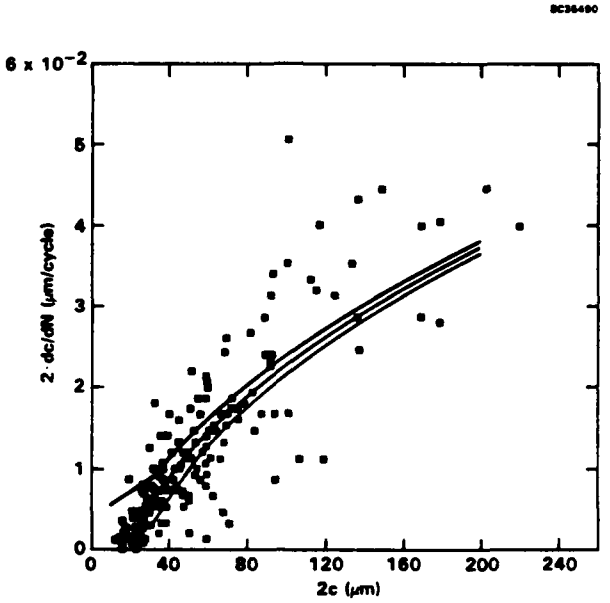

Fig. 3 As for Fig. 2, but with the predicted curves calculated according to Model 2 of Refs. 1 and 3.

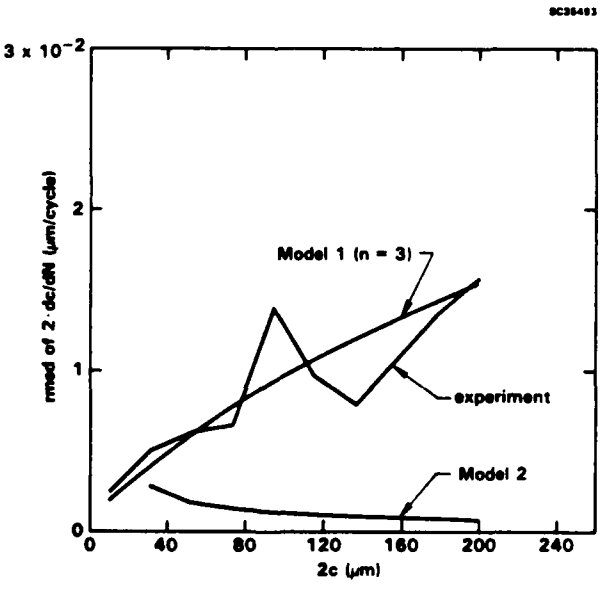

Fig. 4 Irregular curve: the rmsd of the velocity data of Fig. 2, calculated according to Eq. (10). Smooth curves: the rmsd of the crack velocity calculated using Model 1 (n = 3) or Model 2, as marked.

$$\sigma_v^2(c_j') = \frac{1}{N_j} \sum_{i \text{ in } b_j} \left[\frac{V_i - v(c_i, Eu)}{v(c_i, Eu)}\right]^2 , \qquad (10)$$

where the sum is restricted to the data for which $2c_i$ falls in b_j, which is satisfied for N_j points. Note that the predicted rmsd's for n = 1 and n = 10 in Model 1 are virtually the same as that shown for n = 3.

Inspection of the data shown in Fig. 2 suggests that a threshold for growth may exist for cracks less than 10 μm at the stress level used in the experiment. The data for dc/dN perhaps tend to zero to the right of the origin, even though the shortest cracks observed were still propagating. This possibility was investigated by subtracting a constant threshold stress intensity factor from the bracketed terms on the right hand side of Eq. (1), with the understanding that v(c,u) vanishes if the sum of the bracketed terms is negative. It was found that the average velocity dipped as expected for $2c \leq 20$ μm, without any conclusive effect on the measure S (Eq. (8)) of the goodness of fit. All other conclusions were unaffected by this small threshold.

3.0 MONTE CARLO SIMULATIONS OF SMALL FATIGUE CRACK GROWTH

In this section will be described Monte Carlo simulations of two-dimensional small cracks propagating under mode I cyclic loading across a plane section of a stochastic microstructure. Some observations on the importance of the simulations are noted in Section 3.1. The essential physics being represented in the simulations are outlined in Section 3.2. The derivation of an efficient, approximate algorithm for estimating the mode I stress intensity factor K_I around a plane, irregular crack is presented in Section 3.3. The generation of a two-dimensional (plane section) stochastic microstructure is described in Section 3.4; and algorithms for simulating the advance of an irregular crack front across it are described in Section 3.5. The definitions of physically significant statistics characterizing the stochastic growth of two-dimensional cracks are given in Section 3.6, together with an illustration in which some data on the aspect ratios of small surface cracks in Al 7075-T6 are compared with Monte Carlo simulations.

3.1 The Role of the Monte Carlo Simulations

The analysis of small crack data for Ti 6-2-4-6[1,3] led to the interesting conclusion that, for cracks of 5-20 grain diameters (50-250 μm) in that material, fluctuations in the surface crack velocity, 2dc/dN, depend only on the local surface microstructure. When this is the case, fatigue lifetime prediction is greatly simplified, since surface observations alone, in conjunction with stress analysis accounting for the extrinsic effects of part shape and stress state, will provide sufficient information on which to base a probabilistic model. However, for cracks spanning just one or two grains (which may be hundreds of microns in some materials), a more complex situation should be anticipated, since there is then likely to be strong correlation between the rates of advance of surface and subsurface segments of the crack front. To address the transition between these regimes, a very detailed and flexible model is required of a two-dimensional small crack growing through a stochastic microstructure. By far the most convenient format for such a model is Monte Carlo simulations, which are described in this section and Refs. 6 and 7.

A second important task for the Monte Carlo simulations is to provide an assessment of the accuracy of various treatments of the phenomenon of intermittent crack arrest, which is now known to be common, if not ubiquitous, in small crack growth

in alloys (see references cited in Ref. 8). Observations of naturally occurring surface cracks in Al alloys, Ti alloys, steels, and Ni-based superalloys have revealed that the surface tips of such cracks are frequently arrested when they reach grain boundaries. Propagation resumes after some further fatigue cycles, whose number depends on crack length and stress level, as well as local, stochastic microstructural factors such as grain size.[9] From the point of view of constructing a probabilistic model of crack growth subject to this phenomenon, it must be understood that intermittent crack arrest makes necessary a state space of increased dimensionality if the stochastic growth is to be represented as a Markovian process. It is no longer sufficient to describe the state of a crack by its length alone, because the probability that the crack has a certain length at a certain time is not dependent solely upon the length it had at a prior time, which is the Markovian condition. To recover a Markovian process, it is necessary to consider explicitly the possibility that between the two epochs the crack (or some portion of the crack front) has been and possibly remains temporarily arrested. The elapsed duration of such an arrest must be described by an additional state variable. A probabilistic model with such an expanded state space has been presented in Ref. 8 (work under a prior contract) for the case where the propagation of a small surface crack can be described solely in terms of the visible surface tips and the surface microstructure they encounter. The Monte Carlo simulations reported below provide an even more general description of intermittent arrest, because each segment of the entire crack front is individually represented as either propagating or temporarily arrested. Therefore, the Monte Carlo simulations provide a sufficient background against which to test the accuracy of various assumptions and approximations inherent in simplified probabilistic models couched in state spaces of reduced dimension.

Aside from the questions raised when fatigue crack growth is intermittent, the Monte Carlo simulations are also capable of generating large, detailed data bases against which simpler probabilistic models can be tested. This role will be discussed further in Section 4.

3.2 The Essential Physics Underlying the Simulations

There are several mechanisms related to microstructure that can cause small crack propagation to depart from the predictions of linear elastic fracture mechanics (LEFM) or, in other words, destroy similitude with the propagation of large cracks when

dc/dN is plotted as a function of ΔK. The mechanisms include temporary arrest at grain boundaries, deceleration caused by back stress or fracture surface roughness, acceleration caused by enhanced local plasticity, and fluctuations in the local stress field caused by elastic inhomogeneity and anisotropy. In each case, the strength of the effect of these mechanisms depends on the size, orientation, and mechanical properties of the grains in the immediate vicinity of the crack front. This knowledge is based exclusively on observations of fluctuations in dc/dN for the visible surface manifestation of small cracks, together with detailed records of the surface microstrucure through which the crack tips are propagating. However, it is very reasonable to hypothesize that the same or at least similar mechanisms are also affecting the propagation of subsurface segments of the crack front, with the pertinent microstructural factors being the size, orientation, and mechanical properties of invisible, subsurface grains. In that case, the microstructure-based modifications to the crack driving force will fluctuate around the crack front in concert with fluctuations in the microstructure. The stochastic microstructure will thus cause fluctuations in the local rate of advance of different segments of the crack front, and the crack front must become irregular. It is the purpose of the Monte Carlo simulations to quantify such irregularity, and relate it directly to laws of growth hypothesized or determined empirically to represent the effects of the microstructure.

The tendency of the stochastic microstructure to make the crack front irregular is balanced by the dependence of the stress intensity factor on crack shape. For example, for an embedded irregular plane crack, the mode I stress intensity factor, K_I, is generally reduced on protrusions and enhanced on retarded segments, so that, in the absence of microstructural fluctuations, the crack always tends to be circular. For a surface breaking crack under mode I loading, the equilibrium shape is approximately a smooth semi-ellipse of aspect ratio 0.4.

The degree of irregularity expected for any small crack will therefore be determined by the relative strengths of the disordering microstructural effects and the smoothing shape dependence of K_I. Since K_I can be calculated, the laws purporting to describe microstructural effects can be tested by measuring the degree of irregularity. Note that as the small crack grows into a large crack, the role of the microstructure diminishes, and the crack will generally be driven by K_I to be smooth.

3.3 Approximate, Fast Algorithm for K_I

The feasibility of the Monte Carlo simulations depends critically on being able to estimate K_I very quickly for plane cracks of arbitrary shape. Exact calculation of K_I would be prohibitively slow and, therefore, simple approximations to K_I have been derived.

3.3.1 Approximation for K_I Around an Embedded Crack

The approximation for K_I around an embedded crack is based on estimates $K_I^P(\alpha)$ of K_I at the zenith, P, of a protrusion, and $K_I^Q(\alpha)$ at the nadir, Q, of a retarded segment, where α is the half-angle subtended by either feature at the center of the crack. Both the protrusion and the retarded segment considered have the square-shouldered geometry shown in Fig. 5. The uniform applied tensile stress has value σ_∞.

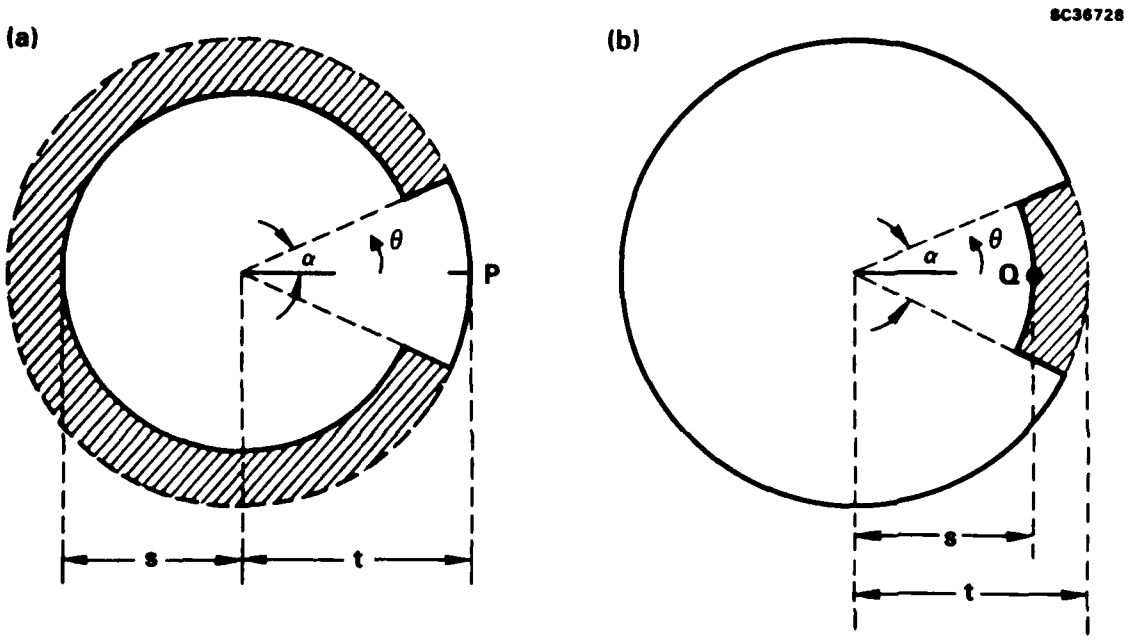

Fig. 5 The geometries of (a) the protrusion and (b) the retarded segment used to estimate K_I at the extrema of an irregular plane embedded crack.

3.3.1.1 $K_I^P(\alpha)$ at the Zenith of a Protrusion

$K_I^P(\alpha)$ was estimated by calculating the reduction from $K_I^t = 2\sigma_\infty\sqrt{t/\pi}$ for a circular crack of radius t generated by closing most of the crack down to radius s (see Fig. 5a). The normal surface tractions required to close the part of the crack shaded in that figure were approximated by the stress field that exists outside a loaded crack of radius s, given analytically by Sneddon.[10] The estimate of K_I^P is then obtained by integrating over the shaded area the product of Sneddon's stress field and the Green's function for the penny crack in a homogeneous, isotropic material obtained by Smith et al.[11] Thus,

$$K_I^P(\alpha) = 2\sigma_\infty\sqrt{t/\pi} - \int_{s/t}^{1} \frac{4\sigma_z(r)}{(\pi t)^{3/2}\sqrt{1-\rho^2}} \{\tan^{-1}[\tfrac{1+\rho}{1-\rho}\tan(\pi-\tfrac{\alpha}{2})] - \tan^{-1}[\tfrac{1+\rho}{1-\rho}\tan\tfrac{\alpha}{2}]\}\, t^2\rho d\rho \quad , \tag{11}$$

where $\rho = s/t$ and

$$\sigma_z(r) = \frac{2\sigma_\infty}{\pi}\left[\sin^{-1}\frac{s}{t} - \frac{s}{\sqrt{r^2-s^2}}\right] \quad . \tag{12}$$

When $\alpha = 0$, this expression is exact. Equation (11) then yields zero for all values of s and t, since, when the crack is closed between s and t, there is no longer a singularity at r = t. When $\alpha > 0$, $\sigma_z(r)$ of Eq. (12) is in fact insufficient to close the crack at any point for which $r < t$. This can be seen by observing that, if the remanent crack opening displacement were exactly zero over some surface of $(s < r < t, \alpha < \theta < 2\pi-\alpha)$ (where θ is the angular variable defined in Fig. 5) and nonzero elsewhere, then some derivative of the nonnegative displacement field must have a discontinuity for $s < r < t$. This is impossible because all the derivatives of the field $\sigma_z(r)$ of Eq. (12) are continuous over $s < r < t$. Nevertheless, the results given below show that the displacement is probably small except near $\theta = \alpha$ (the edge of the protrusion), and therefore the approximation should be reasonable.

Normalized to $2\sigma_\infty\sqrt{t/\pi}$, K_I^P is independent of t. Because of the singularity in the integrand of Eq. (11) at $\rho = 1$, which arises from the Green's function, it is not an

adequate approximation to replace $\sigma_z(r)$ of Eq. (12) by the asymptotic form $A(r-s)^{-1/2}$, even for $s \simeq t$. The integral of Eq. (11) may be evaluated conveniently by cubic spline integration after removing the singularities at $\rho = s/t$ and $\rho = 1$ by the substitution $\sin^2 u = \frac{\rho - s/t}{1 - s/t}$.

$K_I^P(\alpha)/(2\sigma_\infty \sqrt{t/\pi})$ is shown in Fig. 6. It is significantly reduced from unity only at small α (tens of degrees), even when $s = 0$. Further calculations show that 80% of the reduction is generated by the surface forces applied within $\pi/3$ of the protrusion for all values of s/t and $\alpha \leq \pi/2$. In other words, the protrusion is only weakly influenced by the more distant periphery of the crack.

Numerical calculations show that $K_I^P(\alpha)$ evaluated according to Eq. (11) is well approximated for $s/t > 0.5$ by

$$K_I^P(\alpha) \simeq 2\sigma_\infty \sqrt{t/\pi} \cdot \frac{2}{\pi} \tan^{-1} \left[\frac{3 + s/t}{1 - s/t} \tan \frac{\alpha}{2}\right] \quad . \tag{13}$$

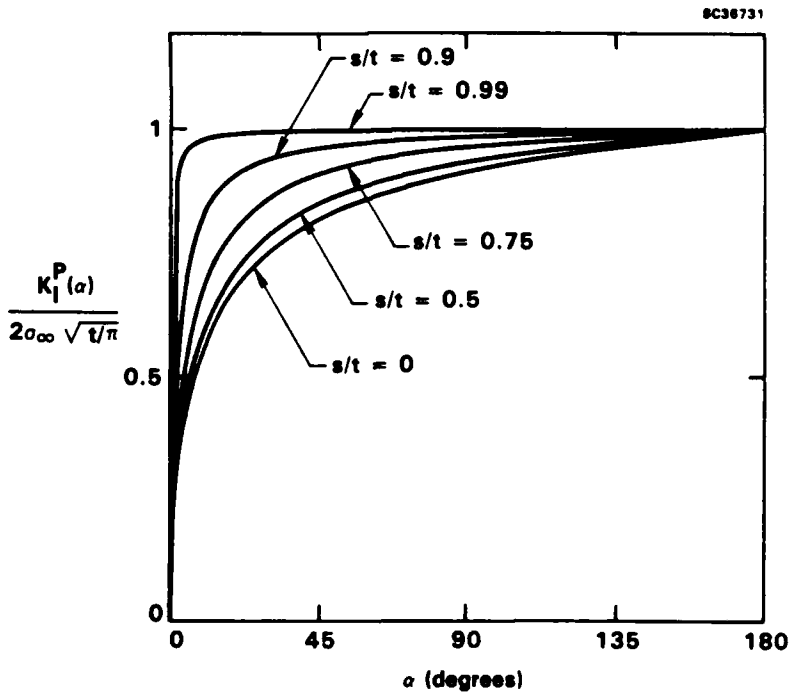

Fig. 6 $K_I^P(\alpha)$ normalized with respect to K_I for a penny crack of radius s, as a function of s/t.

3.3.1.2 $K_I^Q(\alpha)$ at the Nadir of a Retarded Segment

A similar argument was used to estimate K_I^Q. The surface tractions required to close down the fracture surfaces of a loaded crack over the area shaded in Fig. 5b can be related by an integral equation[12] to the normal displacement of the original penny crack of radius t. If the required stress field is assumed to be independent of the polar angle θ, which is a fair approximation when evaluating $K_I^Q(\alpha)$ at the center of the retarded segment, then the integral equation is one-dimensional and easily solved numerically as follows.

The normal displacement along $\theta = 0$ of a penny crack of radius t subjected to surface tractions $\sigma_z(r)$ over $-\alpha \le \theta \le \alpha$ is given by

$$u(x) = \frac{4(1-\nu^2)}{\pi E} \int_x^t \frac{1}{c'^2\sqrt{1-x^2c'^2}} \int_0^{c'} \frac{c'\sigma_z(r)\, h(x/c', r/c', \alpha) r dr}{\sqrt{1-r^2/c'^2}}\, dc' \quad , \tag{14}$$

where ν is Poisson's ratio, E is Young's modulus, and

$$h(p,q,\alpha) \equiv \frac{1-p^2}{2\pi^2} \int_0^{2\pi} \frac{\tan^{-1}\left[\frac{1+q}{1-q}\tan\frac{\alpha-\theta}{2}\right] - \tan^{-1}\left[\frac{1+q}{1-q}\tan\frac{-\alpha-\theta}{2}\right]}{1-2p\cos(\theta-\alpha)+p^2}\, d\theta \quad . \tag{15}$$

The function h is readily computed, stored, and evaluated subsequently by interpolation, since $0 \le h \le 1$.

If u(x) in Eq. (14) is made equal to the opening displacement of the original penny crack under load σ_∞, i.e.,[10]

$$u(x) = \frac{4(1-\nu^2)\sigma_\infty}{\pi E}\sqrt{t^2-x^2} \quad ; \tag{16}$$

and one writes $\sigma_z(r) = \Sigma_z(r)/(r-s)^{1/2}$ to introduce explicitly the expected singularity at Q, then Eq. (14) becomes a straightforward integral equation in $\Sigma_z(r)$; and

$K_I^Q(\alpha) = \Sigma_z(s) \cdot \sqrt{2\pi}$. The integral equation is solved by guessing $\Sigma_z(r)$, and iterating by some heuristic algorithm until self-consistency is achieved. Further numerical calculations then show that, to a good approximation for $s/t \leq 0.5$,

$$K_I^Q(\alpha) \simeq 2\sigma_\infty \sqrt{s/\pi} / \{\frac{2}{\pi} \tan^{-1}[\frac{3+s/t}{1-s/t} \tan \frac{\alpha}{2}]\} \quad . \tag{17}$$

3.3.1.2 Embedded Plane Cracks of Arbitrary Profile

For crack fronts of arbitrary profile, the half-width α of a protrusion or retarded segment is defined as half the angle between the points on either side of the extremum in question at which the radius of the crack was equal to its average radius (Fig. 7a). The value of K_I between the zenith of a protrusion and the nadir of a retarded segment is then written simply as

$$K_I(\theta) = [(r(\theta) - s)K_I^P + (t - r(\theta))K_I^Q]/(t - s) \quad , \tag{18}$$

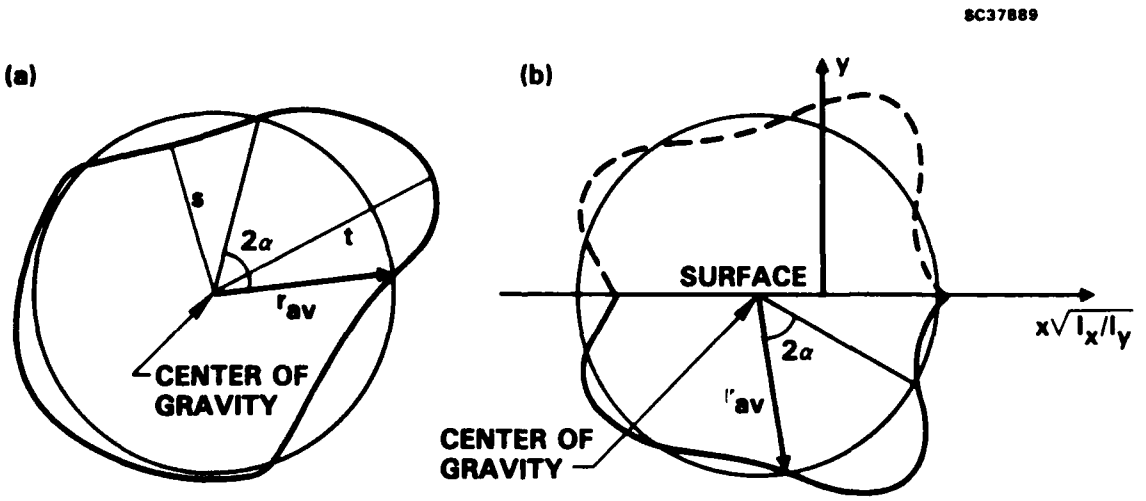

Fig 7 Illustrating the procedures used to define protrusions and retarded segments on an irregular crack for the purpose of invoking Eqs. (13), (17), and (18).

where $r(\theta)$ is the radius of any point relative to the center of gravity of the crack, and s and t are defined in Fig. 7a.

Now square-shouldered protrusions or retarded segments, such as those on which the estimates of K_I^P and K_I^Q were based, almost never occur in natural fatigue cracks, because K_I vanishes at the apex of a square feature that locally leads the crack front and diverges at such points that locally trail the crack front. Because of this and the approximations from which Eqs. (11) and (14) were derived, the identification of α for a smooth rather than square-shouldered feature is subjective. Therefore, the term $\alpha/2$ in Eqs. (13) and (17) was replaced by $\pi/2 \cdot \alpha/\alpha_o$, with the parameter α_o evaluated by calibration against K_I for elliptical cracks.

The exact results for an elliptical crack[13] with $s \approx t$ can be fitted perfectly by Eq. (18) by adjusting α_o. With this value of α_o retained for all cases (viz., $\alpha_o \approx 0.201$, found by fitting to K_I for an ellipse having $s/t = 0.99$), the agreement with other known solutions is as illustrated in Fig. 8. Even for protrusions and retarded segments of significant magnitude ($s/t \sim 0.5$), the approximation is always accurate to within a few percent. Of course, the near agreement at the sharp points of cases (d), (e), and (f) is fortuitous, since K_I should really vanish there, and both the approximation and the numerical results of Mastrojannis et al[14] are in error in this regard. However, this is an unimportant shortcoming, because extremely sharp features are not found in natural cracks.

Most importantly for the present application, the approximation gives fair estimates of both the dependence of K_I on α and its relative magnitudes at smooth extrema on the same crack. These are the properties essential to balancing the tendency of $K_I(\theta)$ to make a crack regular against the disruptive effects of the microstructure. Note that K_I^Q is correctly predicted to diverge and K_I^P to vanish as $\alpha \to o$. This implies that very sharp irregularities of the crack front will not be found.

3.3.2 K_I on Surface-Breaking Cracks

Convenient algorithms have been given by Newman and Raju for estimating K_I around semi-elliptical surface cracks in rectangular beams of width 2b and depth t under remote uniform tension σ_∞ and remote bending stress S_b.[15,16] If 2c is the crack's length on the surface and a its depth, then for $2c \geq a$,

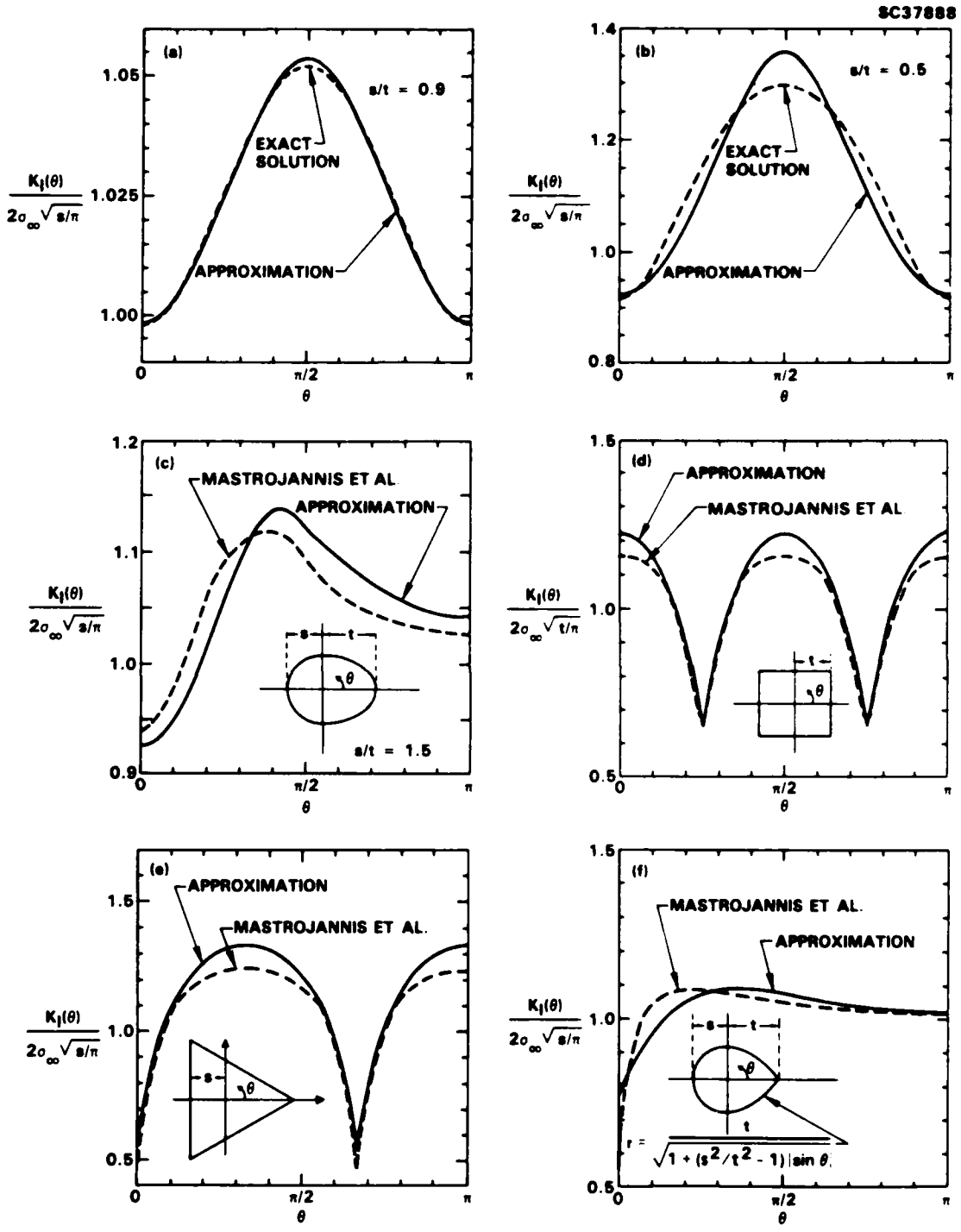

Fig. 8 Testing the algorithm of Eqs. (13), (17), and (18) for embedded cracks against known solutions for embedded irregular cracks: (a) and (b) are for ellipses with semi-axis as marked; the shape of the cracks in (c)-(f) are shown in insets.

$$K_I(\phi) = (\sigma_\infty + H_s S_b) \frac{\sqrt{\pi a}}{E(k)} F(\frac{a}{c}, \frac{a}{t}, \frac{c}{b}, \phi) \quad , \qquad (19)$$

where E is the complete elliptic integral of the second kind; $k^2 = 1-a^2/c^2$; F is a polynomial in a/c, c/a, a/t, and c/b, and a simple trigonometric function of ϕ, the parametric angle of the ellipse; and H_s, the bending multiplier, is a simple algebraic function of a/t, a/c, and $\sin\phi$.

To account for departures of the crack front from the semi-elliptical shape, Eq. (19) was combined with Eqs. (13), (17), and (18) by the following ansatz. The center of mass and the moments of inertia I_x and I_y of an irregular crack were found, and taken to define the center and semi-axes ($c = 2\sqrt{I_y}$ and $a = 2\sqrt{I_x}$) of a smoothing semi-elliptical crack. The x axis was rescaled by the factor a/c, so that the fitted semi-elliptical crack would become a semicircular crack, and the mirror image was added (Fig. 7b) to generate an entire irregular, approximately circular crack. Equation (18) was then used to generate values of $K_I(\theta)$ around this scaled crack, normalized to $K_I(a) = 2\sigma_\infty\sqrt{a/\pi}$. These normalized values of $K_I(\theta)$ represent the relative acceleration and retardation of local protrusions and retarded segments. These values were then multiplied by the results of Eq. (19) for the semi-elliptical crack of semi-axes c and a, to account for gross shape and size effects.

The quality of the results generated by this procedure was then tested by comparison with the essentially exact numerical solutions of Gyekenyesi and Mendelson[17] for a rectangular surface crack in a finite rectangular slab. In Ref. 17, calculations were made for a crack embedded in a slab whose depth and width in the crack plane were as shown in the insets of Fig. 9, and whose length normal to the crack plane was also finite (3.38c), whereas Newman and Raju have supplied expressions (Eq.(19)) for bars of infinite length only. With the understanding that this might detract from the fairness of the test, the comparison of the results of Ref. 17 and the present approximate algorithm is presented in Fig. 9. Despite the fact that the rectangular surface crack is an extreme shape and therefore a severe test, the agreement is reasonable except for the case of very low aspect ratio (a/2c = 0.15), and even there the qualitative trends are faithfully reproduced. Considering that the present algorithm will always tend correctly to Newman and Raju's standard expressions (Eq.(19)) as the crack shape tends to semi-elliptical, and that

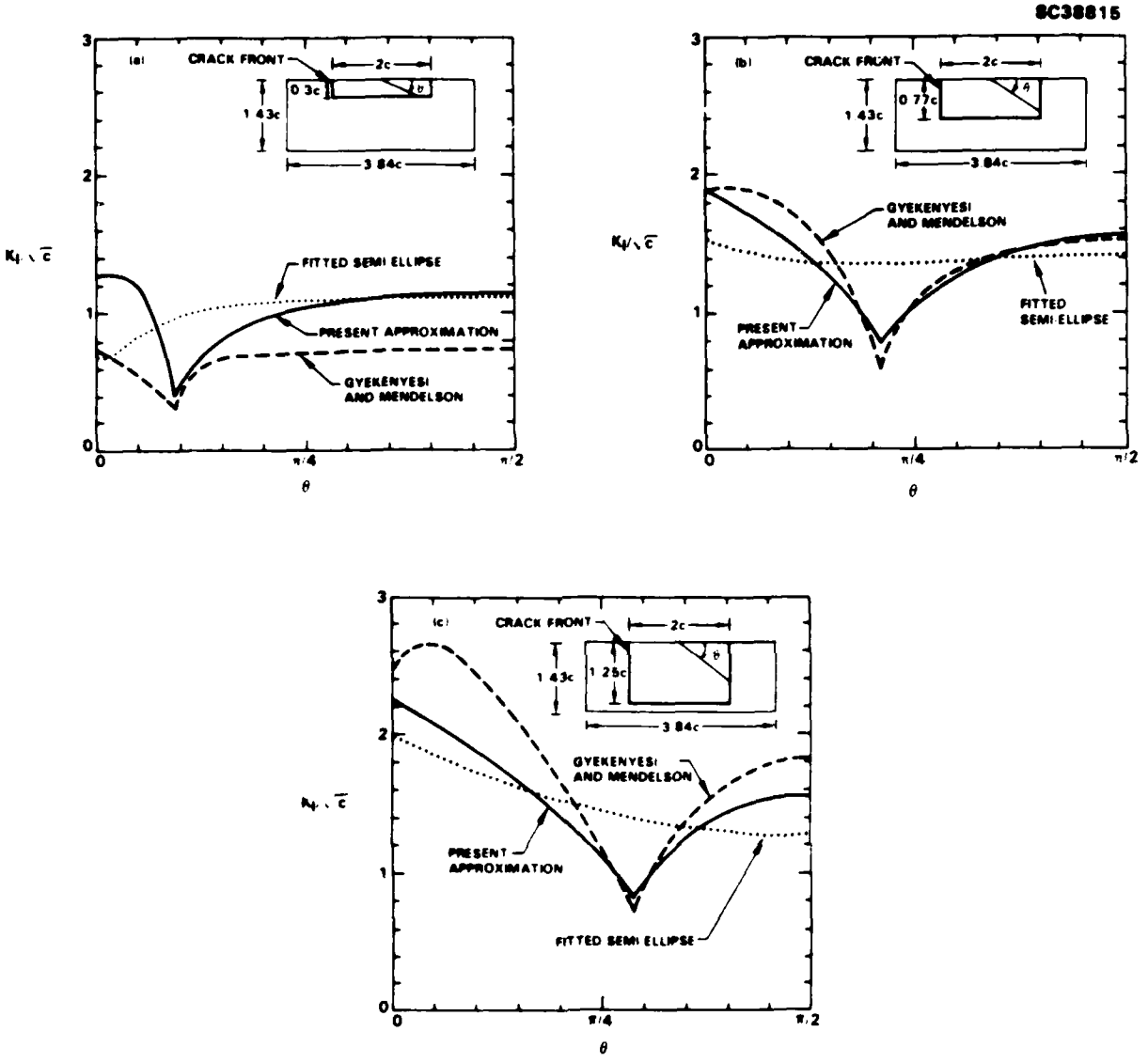

Fig. 9 Testing the algorithm of Eqs. (13), (17), (18), and (19) for surface cracks against the calculations of Gyekenyesi and Mendelson[17] for rectangular cracks in finite rectangular bars. The insets show the dimensions of the cases considered. All values of K_I are normalized to $\sqrt{c}$, where 2c is the surface crack length. The curve marked 'fitted semi-ellipse' (dotted line) in each case shows the results of Eq. (19) for a semi-elliptical crack having the same moments of inertia as the rectangular crack.

crack fronts generated in the simulations and found naturally are generally fairly smooth and not far from semi-elliptical, the approximate algorithm is adequate for the applications reported below.

3.4 The Generation of Random Microstructures

A single instance of a stochastic microstructure is generated as follows. Nucleation sites of a prescribed average density are placed on the plane of the crack in a Poisson process (i.e., with no correlation in their locations) by invoking a pseudo-random number generator. The grain boundaries are then determined by the Wigner-Seitz construction, which defines each grain as the area bounded by the perpendicular bisectors of the lines joining that grain's nucleation site to the nucleation sites of all its contiguous neighbors. The resulting cellular structure, an example of which is shown in Fig. 10, is a set of Voronoi, Dirichlet, or Wigner-Seitz polygons. All the polygons have straight edges, at least three neighbors, and are convex. The average grain size is established by the prescribed density of nucleation sites. There is some correlation between the sizes of adjacent grains, with large (small) grains tending to have large (small) neighbors. This correlation is often expressed in terms of the number of sides of the polygons, but it also exists for their areas. The extensive literature on random Voronoi polygons may be conveniently entered through Refs. 18-20.

There are some characteristics of Voronoi polygons that are unrealistic in the context of metal or alloy microstructures. For example, there are numerous very small grains, which would probably be subsumed in an alloy by larger neighbors during annealing, and the straight-edged polygons are unnaturally smooth, since natural grain boundaries are generally faceted and otherwise irregular. However, the dependence of the laws of crack growth on local microstructure does not usually involve such geometrical details. The laws of growth refer perhaps to the average grain size in the vicinity of a segment of the crack front, or some crude measure of local slip distances. Therefore, Voronoi polygons are, to the best of current knowledge, quite acceptable for the Monte Carlo simulations. Note that nonequiaxed grain structures can be generated simply by rescaling one of the axes.

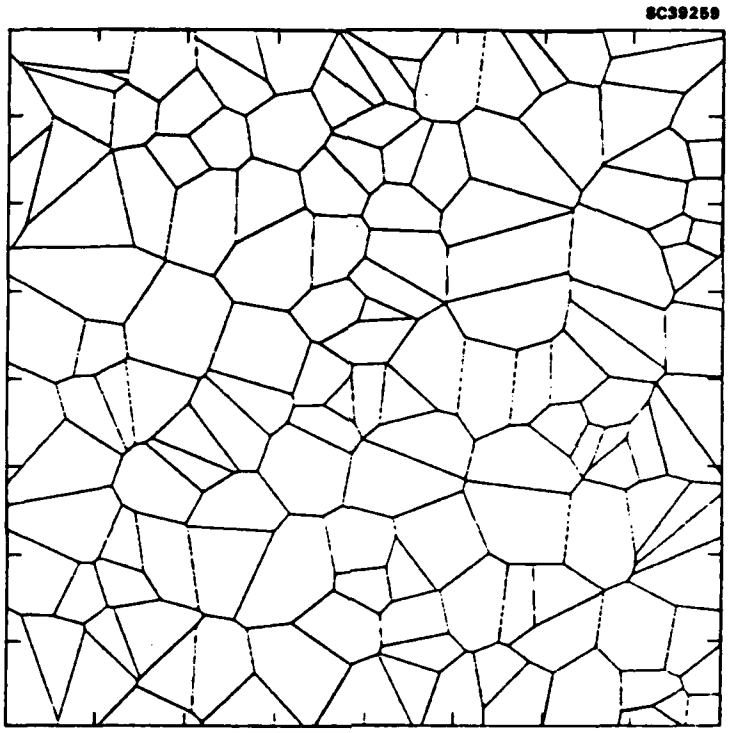

Fig. 10 A typical random microstrucure consisting of Voronoi polygons.

The procedure followed to execute the Wigner-Seitz construction was as follows. For a given nucleation site, i, the grain enclosing it was first supposed to be the entire, usually rectangular, area A within which crack growth was going to be simulated. For every other nucleation point, j, lying within a cutoff distance, d_c, of site i, the perpendicular bisector was formed, and the question asked of whether it intersected the polygon currently recorded as surrounding site i. If so, the polygon was reduced to include the appropriate interval of the bisector as a new side. This was repeated for all sites j within d_c of site i, and then for all sites i. The area A must always be chosen large enough that an embedded crack never reaches the boundary region during a simulation, because this implementation of the Wigner-Seitz method is affected by the external boundaries of A: unusually large grains are formed there. When required, a free specimen surface was formed by deleting all grains and parts of grains lying beyond a line drawn across area A, just as though the specimen had been physically cut.

To enable convenient reference to the information contained in a given microstructure, a discrete square grid was defined on the plane of the crack. Each point on

this grid was then associated with the number of the grain containing it and with other measures of the local microstructure. For example, for modeling crack growth in Al alloys, an appropriate measure upon which plasticity-induced closure depends is the distance from the grid point to the next grain boundary measured along the line emanating from the center of the crack. Other characteristics, such as grain orientation, might be preferred for other materials.

3.5 Initiation and Propagation of a Crack Front

The simulation of fatigue crack initiation can be treated according to various models. Depending on the known mode of initiation and the stage of crack growth under study, one might begin with a crack that spans several grains, or extends exactly to the boundaries of just one grain, or is smaller than a single grain, or even vanishingly small. For crack fronts that are not assumed to coincide initially with a grain boundary, the aspect ratio and shape remain to be prescribed. For naturally initiated cracks, it is frequently the case that initiation occurs mainly in unusually large grains. The appropriate initiation model that takes all such factors into account must be chosen for each application of the Monte Carlo simulations.

A Monte Carlo simulation begins by generating a random, two-dimensional pattern of grains lying on the plane of growth, as described in the preceding section. The initial crack is introduced according to the initiation model. The crack front after N_i cycles (beginning with $N_1 = 0$) is represented as a sequence of straight line segments meeting at the vertices $\{(x_j,y_j)\}$. The applied cyclic mode I stress intensity factor, $\Delta K_I^{(j)}$, corresponding to the prescribed external stress range, is calculated at each vertex j according to the algorithms derived in Section 3.3. The microstructural environment of the vertex j can be found immediately by identifying the element of the square grid (see Fig. 11) in which (x_j,y_j) lies, and referring to the corresponding elements in the stored tables of microstructural parameters for the current microstructure. $\Delta K_I^{(j)}$ (or $K_{min}^{(j)}$ and $K_{max}^{(j)}$) and the microstructural parameters for vertex j are then supplied to a subroutine that invokes the prescribed laws of crack growth for the given simulation. The output of that subroutine is the velocity, v_j, of the crack front at the vertex j.

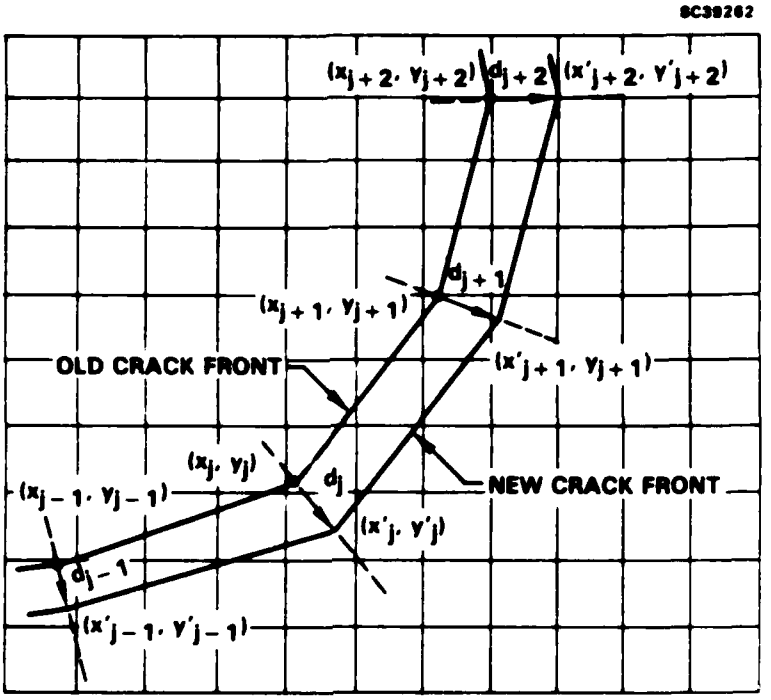

Fig. 11 Illustrating the algorithm for advancing the crack front. The square grid marks the discrete elements within each of which the microstructural parameters (e.g., size of the grain containing the element, or the distance of the element from the next grain boundary) are taken to be constant.

The crack front after N_{i+1} cycles is found by assuming that it advances in the direction of the normal to the front at every point. At each vertex, this direction is taken to bisect the angle between the two adjacent straight segments (Fig. 11). The distance over which vertex j advances is just $v_j(N_{i+1}-N_i)$. The step length $N_{i+1}-N_i$ is chosen to be small enough that the simulation is independent of it. This entire process amounts to first-order integration of a set of coupled differential equations governing the advance of the vertices of the crack front according to the prescribed laws of growth.

The number of vertices on the crack front is chosen initially to be large enough that each segment is small relative to the scale of the microstructure. This condition is maintained as the crack grows by adding a new vertex at the midpoint of any segment that exceeds some critical length.

Because cracks tend to grow faster as they get bigger, it is usually convenient to control the maximum or average of the distances of advance, d_j, during each incre-

ment of cycles, rather than choosing N_{i+1}-N_i to be constant. In this way, the spacing between successive calculated crack fronts can be kept small relative to the microstructure.

The propagation of surface cracks growing according to the Paris law

$$v_j = A(\Delta K^{(j)})^p \tag{20}$$

in the absence of any microstructural effect is illustrated in Fig. 12. Note that memory of the initial value of the aspect ratio disappears by the time the surface length of the crack has increased two- or three-fold, and that the equilibrium shape is approximately, but not exactly or necessarily, semi-elliptical. The velocities v_s of the surface tip and v_b of the bottom of a crack whose shape has reached equilibrium at an aspect ratio a/2c are related by

$$v_b/v_s = a/c \quad . \tag{21}$$

When the velocities are governed locally by the Paris law, it follows that the equilibrium aspect ratio must depend on the parameter p in Eq. (20).

If the laws of growth admit arrest of the crack, then part or all of the crack front may stop growing temporarily or permanently. The state of being arrested is continually monitored as an attribute of each vertex. If all vertices are arrested, then the subroutine containing the laws of growth is interrogated to see whether the arrest is temporary or permanent, based on the existing microstructural environment of the crack front. If arrest is temporary, the record of elapsed cycles is modified and each vertex is freed to propagate as the laws of growth allow. If arrest is total and permanent, the simulation ceases.

When microstructure influences the growth, the crack front frequently develops small, local minima in the crack radius, illustrated schematically in Fig. 13a. The algorithm Eqs. (13), (17), and (18) for estimating K_I generates large values at the nadir of such a narrow retarded segment, because K_I^Q (Eq. (18)) diverges as the half-angle α vanishes. This causes the prediction of an unusually large advance for that part

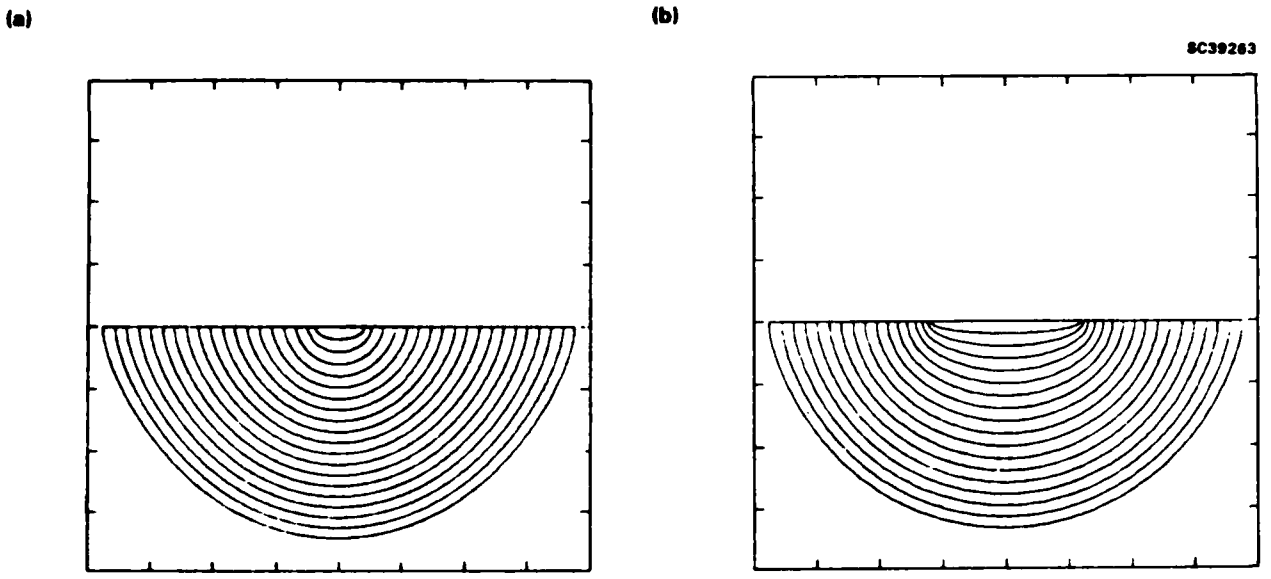

Fig. 12 Propagation of surface cracks according to the Paris law in the absence of microstructural effects starting from a crack of aspect ratio (a) 0.25 and (b) 0.08. The parameter p in Eq. (20) has been assigned the value 2.

of the crack front during a finite increment in elapsed cycles, leading to the false generation of a local protrusion (Fig. 13b). The protrusion in turn generates large values of K_I on either side of it, and a distortion of the crack front similar to the original locally retarded segment occurs on the subsequent iteration (Fig. 13c). This unphysical leapfrogging, which can propagate indefinitely if unattended, can be cut short by identifying the transition from Fig. 13a to Fig. 13b and resetting the crack front along the smoothing dashed line shown in the latter. Note that this needs to be done only if a region of the crack front goes from displaying a retarded segment to displaying a protrusion on one increment of cycles. If there is a persistent microstructural reason for the local change in shape of the crack front, this will still occur over several or many increments of cycles.

When the effects of the microstructure are relatively strong, the crack front becomes highly irregular, and certain topological quirks can arise when calculating the new position of the front according to the algorithm illustrated in Fig. 11. For example,

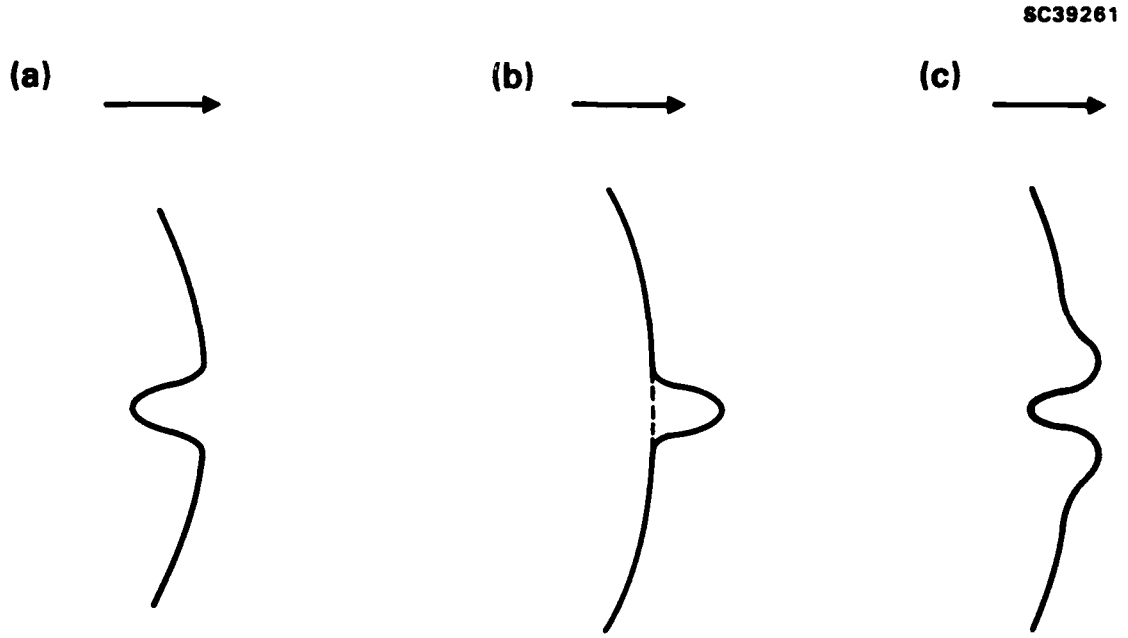

Fig. 13 Leap-frogging caused by a local minimum in the crack radius. (a), (b), and (c) show the same portion of a crack front at successive discrete values of elapsed cycles. The direction of advance of the crack front is indicated by the arrows.

the crack front can form closed loops by crossing over itself, or spurs where it doubles back on itself. The former phenomenon must be excised from the crack front because it quickly leads to numerical explosions in the algorithm for advancing the front; and the latter because it is beyond the scope of the algorithms for estimating K_I. All such aberrations can be readily identified by demanding that the vertices on the front always progress clockwise (or anticlockwise) around the center of mass of the crack, and deleting any vertices that do not.

3.6 Statistics of the Shape and Growth Rate of Small Fatigue Cracks

In this section will be presented a comparison of the measured and predicted statistics of the aspect ratios of small surface cracks in Al 7075-T6, and the definitions of other statistics of shape and growth rate for which experimental data do not yet exist, but could be readily obtained.

3.6.1 Statistics of the Aspect Ratio

A typical simulation of a surface crack is shown in Fig. 14. The grain structure there corresponds to that exposed on a plane cut normal to the rolling direction and normal to the surface of a rolled sheet of Al 7075-T6. The average grain length normal to the rolling direction is ~ 120 μm, and the average depth normal to the surface is ~ 20 μm. After a brief crystallographic phase immediately following initiation, small fatigue cracks in such specimens grow in a transgranular noncrystallographic mode. Plasticity-induced closure causes them to slow down upon reaching each grain boundary and accelerate as each grain is being traversed (Zurek et al[21]). Observations on just the visible surface outlines of individual cracks have led to laws relating the rate of advance of each surface tip to its distance, z, from the next grain boundary. In the simulations shown here, the same law has been assumed to prevail all around the crack front, with z always measured along a line radiating from the original center of the crack. The law has the form

$$\frac{dw}{dN} = A\Delta K^2 \, (1-\beta z/2\bar{r})^2 \, H(1-\beta z/2\bar{r}) \quad , \tag{22}$$

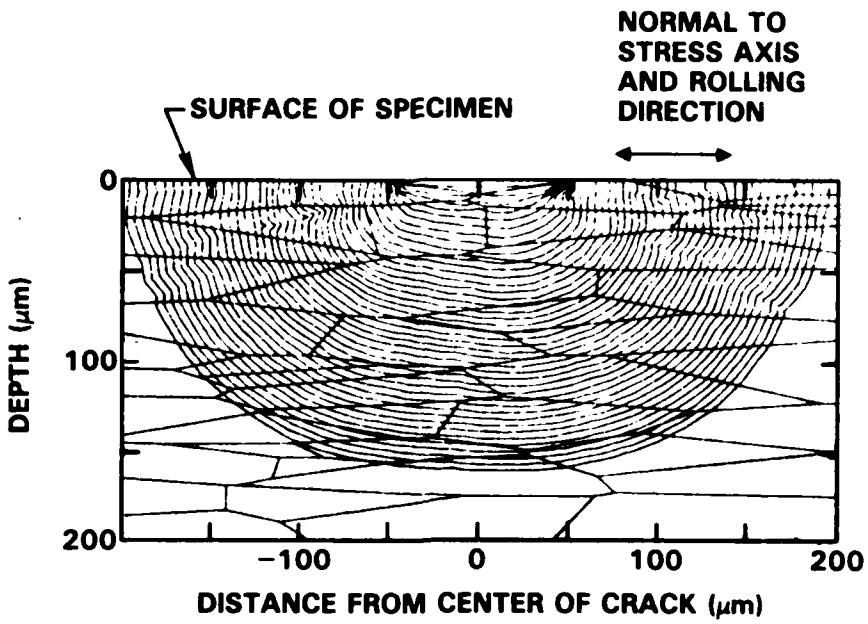

Fig. 14 A simulation of the growth of a surface crack in Al 7075-T6. The position of the crack front is recorded at approximately equal intervals in crack size $\sqrt{ac}$, rather than in cycles.

where w refers to displacement of the crack front along the normal direction, $\bar{r}$ is the average radius of the crack, and β is a parameter whose value for visible surface crack tips in Al 7075-T6 is ~ 0.5. H is the Heaviside step function, and its presence signifies the possibility of part or all of the crack front being arrested by closure. Small cracks in Al alloys are also arrested temporarily by grain boundaries, but this effect is relatively weak in large-grained specimens and it has been ignored here. (Note, however, that grain boundary arrest is readily treated in the simulations, and it will be a principal subject of future studies.)

The simulation shown in Figure 14 exhibits some important general characteristics of small crack growth. When the crack is small relative to the microstructure (less than or equal to a few grains), the crack front can be highly irregular. Parts of it may be arrested by closure (or grain boundary blockage), and the aspect ratio, i.e., the ratio of the average depth to the surface length, fluctuates widely from crack to crack and as the crack grows.

Some statistics of the aspect ratio, defined to be a/2c, where $a = 2\sqrt{I_x}$ and $c = 2\sqrt{I_y}$, are shown in Fig. 15 as functions of the average crack radius, defined as $\bar{r} = \sqrt{ac}$. Both experimental and theoretical data in Fig. 15 were calculated from observations or simulations of many cracks: 16 experimental cracks and 100 simulations. The experimental data were obtained by splitting open specimens after various fatigue exposures and measuring the outline of the fatigue crack front. One striking feature of the experimental data is that many cracks show $a/2c > 0.5$ at $50\ \mu m \leq \bar{r} \leq 100\ \mu m$. This characteristic is reproduced in the simulation (continuous curves of Fig. 15), and can be traced to the fact that the grains are highly nonequiaxed. Values of z tend to be much smaller for those segments of the crack front propagating down into the specimen, and Eq. (22) then implies that a/2c will be augmented. The agreement between the experimental data and the simulations, both in average and deviation, supports the hypothesis that the law of growth obtained from surface observations is also valid for segments of the crack growing down into the bulk.

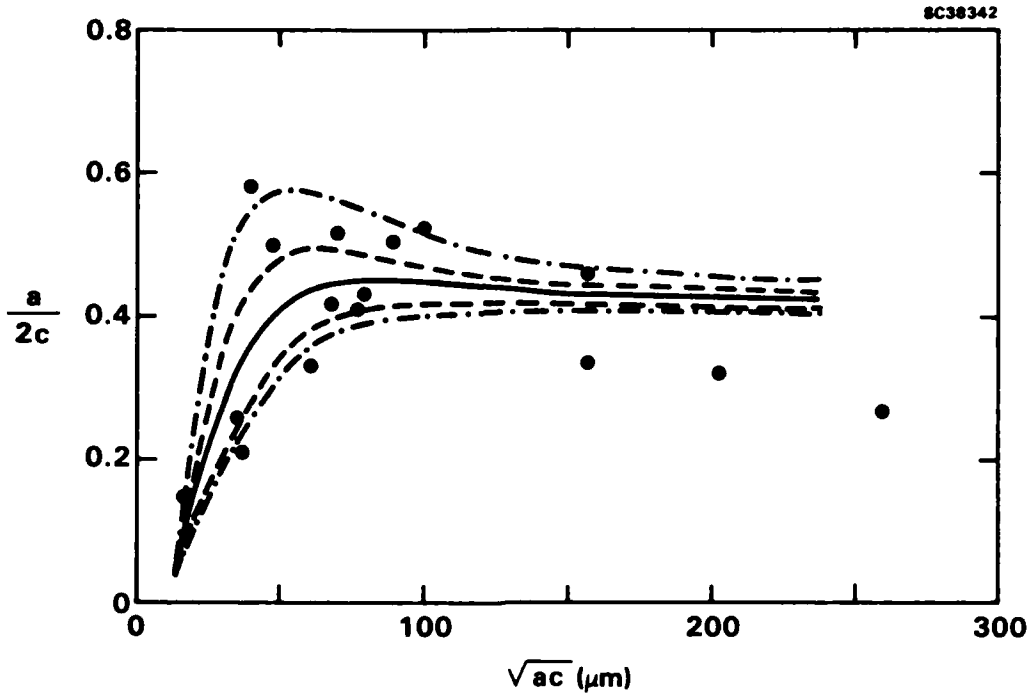

Fig. 15 Aspect ratio of small cracks in Al 7075-T6 as functions of the crack size $\sqrt{ac}$. The data (circles) are for cracks grown at a stress amplitude of 400 MPa. The curves show the distribution of a/2c foun in 100 Monte Carlo simulations. The solid curve shows the average of a/2c in the simulations. The dashed curves should contain 70% and the chain-dot curves 95% of the data.

When the crack spans more than a few grains, the relative strength of microstructural factors decreases, and in the simulations the crack front is restored to its smooth equilibrium configuration, with aspect ratio ~ 0.4, by the variation of $K_I(\theta)$ according to Eqs. (13), (17), (18), and (19). For very small cracks, a/2c is found experimentally to be ~ 0.2. This was mimicked in the simulations by assuming that initiation (e.g., by fracture of stringers of particles or by persistent slip bands forming microcracks) generates relatively long, shallow cracks, about 90 μm x 4 μm. Such an assumption is, of course, testable by appropriate experiments. For the largest cracks, the experimental values of a/2c in Fig. 15 fall below 0.4 because the cracks were grown in bending. The simulations were run before the expressions of Raju and Newman for the bending multiplier in Eq. (19) had been coded.

3.6.2 Other Statistics of the Shape and Growth of Small Cracks

There are many other statistical properties of small cracks that can be conveniently studied by Monte Carlo simulations. These include: (1) the degree of irregularity of the crack front; (2) the covariance between the rates of advance of different segments of the crack front; (3) the persistence of fluctuations in the degree of irregularity or the aspect ratio; and (4) the relationships between either the aspect ratio or the degree of irregularity and the rate of growth averaged around the crack front.

Irregularity may be defined in various ways, and the appropriate definition may depend on the physical mechanisms that generate it. One simple definition is

$$X^2 = \int (1-r(\theta)/\rho(\theta))^2 d\theta / \int d\theta \quad , \tag{23}$$

where $r(\theta)$ is the radial distance from the center of gravity of the crack to the crack front at angle θ, and $\rho(\theta)$ is the equivalent distance for the elliptical crack of semi-axes $c = 2\sqrt{I_y}$ and $a = 2\sqrt{I_x}$. The function X^2 measures the relative departure of the crack from the ellipse of best fit, averaged around the crack front. X^2 is generally largest for small cracks and becomes smaller as the crack grows. The magnitude and rate of decay of X^2, and the covariance between values of X^2 at different times for the same crack, are direct indicators of the strength of the stochastic microstructural factors that tend to disrupt crack growth.

The covariance between the rates of advance of different segments of the crack front (at angles θ and θ') may be defined by

$$\rho_v(\theta,\theta',\bar{r}) = \frac{E\{(v(\theta,\bar{r})-\bar{v}(\bar{r}))\ (v(\theta',\bar{r})-v(\bar{r}))\}}{\sqrt{E\{(v(\theta,\bar{r})-\bar{v}(\bar{r}))^2\}\ E\{(v(\theta',\bar{r})-v(\bar{r}))^2\}}} \quad , \tag{24}$$

where E denotes the expectation value for an ensemble of many cracks, and $v(\bar{r}) = E\{v(\bar{r})\}$, where $v(\bar{r})$ is the rate of growth of a crack of size $\bar{r} \equiv \sqrt{ac}$ averaged around its front. ρ_v is very important to the estimation of remaining fatigue lifetime when experimental observations are limited. For example, NDE of surface cracks generally returns no more information than the visible surface crack length, and perhaps some gross estimate, by acoustic or eddy current measurements, of the size of the invisible

subsurface crack. In the small crack regime, it is then critical to know with what certainty the rate of growth of the subsurface crack can be inferred from the rate of growth of the visible crack. The covariance, $\rho_v(\theta,0)$, obtained from the Monte Carlo simulations using models tested and calibrated by comparing that and other statistics with destructively inspected cracks, provides the answer. Note that a transition in $\rho_v(\theta,0)$ is expected as the crack grows out of the small crack regime. The surface velocity of small cracks will be relatively strongly correlated with the velocity of subsurface segments, because the same microstructural factors may often be affecting both. For larger cracks, the microstructural environment of the surface tips is unrelated to the subsurface microstructure, and $\rho_v(\theta,0)$ will ultimately vanish for $\theta \neq 0$.

The persistence of fluctuations in shape can be quantified by the covariance ρ_x of values of X^2 determined at different times for the same crack:

$$\rho_x(\bar{r}_1,\bar{r}_2) = \frac{E\{(X^2(\bar{r}_1)-E(X^2(\bar{r}_1)))\ (X^2(\bar{r}_2)-E(X^2(\bar{r}_2)))\}}{\sqrt{E\{(X^2(\bar{r}_1)-E(X^2(\bar{r}_1)))^2\}\ E\{(X^2(\bar{r}_2)-E(X^2(\bar{r}_2)))^2\}}} \quad . \tag{25}$$

$\rho_x(\bar{r}_1,\bar{r}_2)$ will generally decay as $\exp[-(\bar{r}_2-\bar{r}_1)/\lambda]$, and the half-life λ, itself a function of $\bar{r}_1$, is a useful measure of both the spatial wavelength of the underlying microstructural disorder and the range of influence of one part of the crack upon another.

One would generally expect the growth rate averaged around the crack front to be strongly correlated with the degree of irregularity. For example, if the role of the microstructure is to retard the crack front locally where it lies in large grains, then a highly irregular crack in which the crack is retarded at several places would usually be propagating slower than a smoother crack front of which no segment is severely retarded. Or, conversely, if the role of microstructure is to cause local acceleration of the front, then the more irregular cracks might be expected to be propagating faster than the average. In either case, comparison of such correlations predicted by simulations with those found by experimental (destructive) measurements of crack shape and velocity would serve as a further direct test of postulated laws of growth. For similar reasons, the average velocity and the aspect ratio can be expected to be correlated. This correlation could be especially useful for predicting remaining lifetime based on NDE measurements, since representative aspect ratios can be measured even for irregular cracks by acoustic methods.

4.0 PROGRAM STATUS AND FUTURE WORK

Following work under this program and a prior DARPA program, our group now possesses models constituting a broad spectrum of the degree of detail that can be incorporated explicitly in probabilistic descriptions of small crack growth. The most explicit models are the Monte Carlo simulations described in the preceding section, which follow all the details of the irregularities of the crack, including intermittent arrest of part or all of the crack front. The next level of detail (i.e., of less detail) is represented by the work under the DARPA program, in which consideration was reduced to the visible surface crack, but allowance was still made explicitly for the non-Markovian nature of growth that is interrupted at grain boundaries. In that work,[8] a Markovian process was recovered by defining an extended state space, which included as independent variables not only the crack length, but also a damage variable that corresponds to the time for which a temporarily arrested crack has been arrested. The least level of detail is represented by the probabilistic model developed in the first year of this program (reviewed in Section 1.2), which comprises the smallest state space that the authors believe is required to make accurate predictions, and retains a simple description of the relationship between stochastic microstructure and the statistics of growth.

One important task for the immediate future is to compare the accuracy of these various models when applied to different materials. In the absence of definitive experimental data (see below), the most effective way to do this is to assume various reasonable modes and laws of growth, set up a rich, synthetic data base using the Monte Carlo simulations, calibrate the simpler models against that data, and then compare the predictions of the simpler models with the corresponding statistics of the synthetic data base. The accuracy must be tested of predictions of: 1) the distribution of times to failure; 2) the distribution of times to failure given the result of an NDE test; and 3) the correlations between rates of growth at different times. At first, this will be done for surface cracks exposed to uniform, fully reversed cyclic loading, to isolate the effects of different treatments of the geometry of the microstructure and temporary arrest of part or all of the crack front. The anticipated transition from strong to weak correlations between surface and subsurface phenomena will be studied, as well as the errors incurred in approximating non-Markovian (intermittent) growth as a Markovian process in a minimal state space.

Both the simple but robust probabilistic model developed in the first year and the Monte Carlo simulations are capable of treating spike overloads and stochastic loading, given some physical model of the dependence of their effects on local microstructure. Unfortunately, there do not yet exist rigorously tested models accounting for overload and load sequence phenomena on the required fundamental level. Therefore, progress will be made by some plausible speculation, based on the understanding gained in our group under other contracts of the evolution of localized plasticity in Al alloys under variable loading.[22-27] For example, according to the models developed for small cracks in Al alloys, the effect of an overload might be either to retard a crack by enhancing backstresses or plasticity-induced closure, or to accelerate it by increasing the local plastic strain range.[27] Which effect prevails depends on the size of the grain containing the various segments of the crack front, and the position of the crack front relative to grain boundaries, including whether the crack front is actively propagating or temporarily arrested at a grain boundary.

The testing of all probabilistic models relies ultimately on the availability of appropriate experimental data in statistically significant quantities. Such data continue to be almost nonexistent for small fatigue cracks. The only data used in this program so far have been acquired in-house, mainly under other programs. All the data for Ti 6-2-4-6 used in Ref. 3 were obtained some time ago under DARPA funding. The data on aspect ratios of cracks in Al 7075-T6 reported in Section 3 were taken under this program in about two days work by breaking open specimens fatigued during another IR&D program. Some data on crack shape and growth rates in Mar-M-246 are expected to be available shortly from a program supported by interdivisional funding from Rocketdyne Division. The most promising small crack data are those currently being generated and collated by a group of ten laboratories in the AGARD program under NATO sponsorship. Unfortunately, those data have not yet been released for general dissemination.

The course of this program has departed slightly from the order in which various tasks were projected to be accomplished in the original work statement (attached as Section 6). The first three items on that list of tasks (spanning the first and second years) have been essentially completed, as has the specification of a process of calibration (Item 5, third year). The models developed so far are all capable of addressing stress overload effects (Item 4, second year). The outstanding work is therefore the untouched parts of Items 4, 5 and 6: considering crack coalescence (Item 4); developing a strategy

for choosing the most advantageous formulation in a given application (Item 5); and evaluating performance under a range of extreme predictive requirements (Item 6). The remaining work in Items 5 and 6 will be the first attacked in the third year, which is about to begin. A serious attempt to treat coalescence requires significant extensions of the models developed so far, and will be deferred until the other tasks have been satisfactorily worked through.

5.0 REFERENCES

1. B.N. Cox and W.L. Morris, First Annual Report on "Integration of Statistical and Physical Models of Short Fatigue Crack Growth," AFOSR Contract No. F49620-85-C-0034, Feb. 1986.
2. B.N. Cox and W.L. Morris, "A Probabilistic Model of Short Fatigue Crack Growth," submitted to Fatigue and Fracture of Eng. Mater. and Structures.
3. B.N. Cox and W.L. Morris, "Model-Based Statistical Analysis of Short Fatigue Crack Growth in Ti 6Al-4Sn-2Zr-6Mo," submitted to Fatigue and Fracture of Eng. Mater. and Structures.
4. M.R. James and W.L. Morris, "Effect of Fracture Surface Roughness on Growth of Short Fatigue Cracks," Met. Trans. A14, 153-5 (1983).
5. K.W. Fertig, "Asymptotic Power of Von Mises Goodness-of-Fit Statistics when Parameters are Estimated," Rockwell International Science Center Technical Report No. SC TR-81-9.
6. B.N. Cox and W.L. Morris, "The Statistics of the Shape of Small Fatigue Cracks," Proc. Fatigue '87, Charlottesville, VA 1987.
7. B.N. Cox and W.L. Morris, "Monte Carlo Simulations of Small Fatigue Crack Growth," in preparation for submission to Eng. Fract. Mech.
8. B.N. Cox, J. Pardee and W.L. Morris, "A Statistical Model of Intermittent Short Fatigue Crack Growth," to be published in Fatigue and Fract. of Eng. Mater. and Structures.
9. W.L. Morris, M.R James and O. Buck, "Growth Rate Models for Short Surface Cracks in Al 2219-T851," Met. Trans. A 12A, 57-64 (1981).
10. I.N. Sneddon, "The Distribution of Stress in the Neighborhood of a Crack in an Elastic Solid," Proc. Roy. Soc., Series A 187, 229-60 (1946).
11. F.W. Smith, A.S. Kobayashi and A.F. Emery, "Stress Intensity Factors for Penny-Shaped Cracks. Part I - Infinite Solid," J. Appl. Mech. 34, 947-52 (1967).
12. I.N. Sneddon and M. Lowengrub, "Crack Problems in the Classical Theory of Elasticity" (Wiley, NY), 1969.
13. M.K. Kassir and G.C. Sih, "Three-Dimensional Stress Distribution Around an Elliptical Crack Under Arbitrary Loading," J. Appl. Mech. 33, 601-11 (1966).

14. E.M. Mastrojannis, L.M. Keer and T. Mura, "Stress Intensity Factor for a Plane Crack Under Normal Pressure," Int. J. Fract. 15, 247-58 (1979).

15. J.C. Newman, Jr. and I.S. Raju, "An Empirical Stress-Intensity Factor Equation for the Surface Crack," Eng. Fract. Mech. 15, 185-92 (1981).

16. J.C. Newman, Jr. and I.S. Raju, "Stress-Intensity Factor Equations for Cracks in Three-Dimensional Finite Bodies Subjected to Tension and Bending Loads," NASA Technical Memo. 85793, April 1984.

17. J.P. Gyekenyesi and A. Mendelson, "Stress Analysis and Stress-Intensity Factors for Finite Geometry Solids Containing Rectangular Surface Cracks," J. Appl. Mech. 44, 442-8 (1977).

18. B.N. Boots, "The Arrangement of Cells in 'Random' Networks," Metallography 15, 53-62 (1982).

19. D. Weaire and N. Rivier, "Soap, Cells, and Statistics - Random Patterns in Two Dimensions," Contemp. Physics 25, 59-99 (1984).

20. D.A. Aboav, "The Arrangement of Cells in a Net. IV," Metallography 18, 129-47 (1985).

21. A.K. Zurek, M.R. James and W.L. Morris, "The Effect of Grain Size on Fatigue Growth of Short Cracks," Met. Trans. A 14, 1697-1705 (1983).

22. W.L. Morris, M.R. James and B.N. Cox, "Fundamental Characterization of Surface Microplasticity," Final Report on NSF Grant No. DMR-8310652, July 1986.

23. W.L. Morris, B.N. Cox and M.R. James, "Investigation into the Fatigue Crack Initiation Process in Metals," Final Report on NADC Contract No. N62269-83-C-0267, Dec. 1985.

24. W.L. Morris, B.N. Cox and M.R. James, "Microplastic Deformation of Al 2219-T851," to be published in Acta Metall.

25. B.N. Cox, W.L. Morris and M.R. James, "Two-Stage Microplastic Surface Deformation in Al 2219-T851," to be published in Acta Metall.

26. W.L. Morris, M.R. James and B.N. Cox, "A Phenomenological Model of the Mechanical Properties of Microplastic Surface Grains During Fatigue," submitted to Acta Metall.

27. M.R. James and W.L. Morris, "The Effect of Microplastic Surface Deformation in the Growth of Small Cracks," in Small Fatigue Cracks, Proc. 2nd Eng. Found. Int. Conf., eds., R.O. Ritchie and J. Lankford, Santa Barbara, CA, Jan. 1986.

6.0 STATEMENT OF WORK

First Year

1. Incorporate models of microstructural short crack growth phenomena into a stochastic damage growth model.

2. Compare model structures of various levels of complexity against synthetic data bases generated principally by Monte Carlo methods.

Second Year

3. Address the formulation and characterization of compound physical/statistical models which account for load history and cyclic stress amplitude.

4. Integrate crack coalescence and stress overload effects into the models.

Third Year

5. Develop a strategy for choosing the most advantageous formulation for a statistical model in a given situation and specify a process of calibration that will optimize predictions of remaining lifetime.

6. Evaluate the performance of predictions made under a range in extremes of predictive requirements.

7.0 PERSONNEL

Dr. Brian N. Cox - Ph.D. in Physics, Monash University (Australia), 1976.

Thesis Title - "A Spherical Cell Model of Metals"

Dr. Winfred L. Morris - Ph.D. in Physics, Northwestern University, 1968.

Thesis Title - "The Nucleation of Gold on Muscovite Mica"

8.0 PUBLICATIONS UNDER THIS CONTRACT

B.N. Cox and W.L. Morris, "A Probabilistic Model of Short Fatigue Crack Growth," (submitted to 'Fatigue and Fracture of Engineering Materials and Structures').

B.N. Cox and W.L. Morris, "Model-Based Statistical Analysis of Short Fatigue Crack Growth in Ti 6-2-4-6," (submitted to 'Fatigue and Fracture of Engineering Materials and Structures').

B.N. Cox and W.L. Morris, "The Statistics of the Shape of Small Fatigue Cracks," to be published in Proc. "Fatigue '87," Charlottesville, VA, June-July 1987.

B.N. Cox and W.L. Morris, "Monte Carlo Simulations of Small Fatigue Crack Growth" (in preparation, probably for submission to Eng. Fract. Mechanics).

9.0 INTERACTIONS AND MEETINGS

Dr. Peter Edwards of RAE, Farnborough, England is the focal point for collaboration and publication of the AGARD small crack data. He has been asked to provide data at the earliest possible date so that the probabilistic models developed under this program can be tested and refined. The AGARD data are believed to comprise many dc/dN vs ΔK curves for individual cracks, fatigued under both Gaussian and spike overload spectra.

A paper on the Monte Carlo simulations will be presented at Fatigue '87 in Charlottesville, June-July 1987.

END

5-87

DTIC